Desalination and Water Treatment
www.deswater.com

doi: 10.5004/dwt.2018.23073

126 (2018) 350–360
September

Synthesis of UiO-66 based on benzoic acid and chloroform with highly efficient adsorption of Congo red dye

Sheng Feng[a,*], Runbai Wang[a], Shanshan Feng[a], Zhihui Zhang[b], Shuguang Liu[a]

[a]*School of Environmental and Safety Engineering, Changzhou University, Jiangsu 213164, China, Tel. +86 519 86330080; emails: shfeng@cczu.edu.cn (S. Feng), ruibaiwang@163.com (R. Wang), fss728@163.com (S. Feng), shguangliu@163.com (S. Liu)*
[b]*Jiangsu Key Laboratory of Advanced Catalytic Materials and Technology, Changzhou University, Jiangsu 213164, China, email: zhangzh@cczu.edu.cn*

Received 8 March 2018; Accepted 28 August 2018

ABSTRACT

In this study, a perfect UiO-66 was synthesized by adding benzoic acid in the precursor solution and activating it with chloroform after synthesis. The crystal morphology and material properties of the synthesized materials were investigated by X-ray powder diffraction, Fourier-transform infrared spectroscopy, scanning electron microscopy, N_2 adsorption–desorption analysis, zeta potential, and thermogravimetric analyses. A typical anionic organic dye, Congo red (CR), was used as the target contaminant to examine the adsorption properties of a series of UiO-66. The acid-promoted and activated UiO-66 had a more regular octahedral structure, high-surface area of 905–1,230 m^2/g, and more positive zeta potential (hydrogen ion), which might explained the greatly enhanced adsorption of CR dye. The effect of several influential parameters such as adsorbent dosage, solution pH, initial dye concentration, temperature, and contact time was well studied and optimized by using batch adsorption study. Moreover, mechanisms with kinetic, isotherm, and thermodynamics were researched in detail. The acid-promoted and activated UiO-66 could be regenerated by a simple N, N-dimethylformamide -washing method and exhibited stable and high reusability over five cycles. Overall, the acid-promoted and activated UiO-66 was an excellent candidate for wastewater treatment due to a simple synthesis procedure, high efficiency, reusability, and stability in the aqueous phase.

Keywords: UiO-66; Acid promotion; Activation; Congo red (CR); Adsorption; Regeneration

1. Introduction

In recent years, organic dyes manufactured by industry for use in products such as textiles, leather, paper, and plastics have been discharged into freshwaters without sufficient wastewater treatment [1–3]. These organic dyes pose a serious threat to human and ecological health, as well as societal values by altering the aesthetics of waterways (e.g., turbidity and color) [4,5]. Due to their complex chemical structure, high stability, and slow biodegradation, organic dye is one of the most difficult chemicals to remove using conventional wastewater treatment processes. Therefore, it is required that innovative, efficient, and scalable methods to remove organic dye pollutants from wastewater.

Compared with the many existing technologies for removing dyes from industrial wastewater, adsorption has long been considered one of the most competitive methods because of simple synthesis, low energy consumption, easy operation, high removal, small amounts of harmful byproducts, and renewable performance. In the adsorption method, it is pivotal to select the appropriate adsorbent. To date, various traditional adsorbents, including silicon nanomaterials [6], clay minerals [7], and activated carbon [8], have many limitations such as low adsorption

* Corresponding author.

capacity, difficulty in recycling, and high cost in the sewage treatment. Consequently, there is need for developing new adsorbents with low cost, high adsorption capacity, and good recyclability.

Metal–organic frameworks (MOFs) represent a new family of microporous materials formed by a network of transition metal ions linked by organic ligands [9]. Due to their characteristic properties of high surface area, high porosity and tunability, MOFs are considered as potential candidates for gas storage, absorption, microelectronics, and catalysis [10–13]. In MOFs family, $Zr_6O_4(OH)_4$ and 1,4-benzenedicarboxylate (H_2BDC) linker forms a 12-coordinate highly packed face-centered cubic structure(the highest reported coordination for an MOF), making the Zr-based MOFs (UiO-66) have unique properties [14], such as a rare water stability, excellent thermal and chemical stability, even in the strong acid and alkali environment to maintain a high stability [15–18]. Because of the water-stable properties and excellent chemical stability in strong acid and alkali environments, UiO-66 has been successfully used in aqueous adsorption. Nevertheless, conventional synthetic UiO-66 has some drawbacks, such as low surface area, small pore size, which affect the adsorption of macromolecular dyes, and the structural defects of UiO-66 affect its hydrophobicity [19]. It is understood that the proper selection of synthesis conditions and activation processes can control and tune the morphologies and textural structures of UiO-66 and result in defect-free UiO-66 in terms of the absence of unreacted benzene dicarboxylic acid linkers into its structure. Li et al. [18] obtained UiO-66 via microwave-assisted synthesis with the addition of acetic acid and demonstrated that the UiO-66 could adsorb charged dyes. Qiu et al. [20] synthesized acid-promoted UiO-66 by using acetic acid or HCl at various reaction conditions and carried out the selective adsorption to anionic dyes (Methyl orange and Congo red [CR]) and cationic dyes (Methylene blue and Rhodamine B). Azhar et al. [21] found that the crystal structure of UiO-66 activated by chloroform was more perfect, and its adsorption performance of sulfonamide antibiotics was greatly improved. In summary, it can be seen that the acid-promoted synthesis and activation processes can effectively improve the crystal structure so as to achieve a better adsorption effect.

In this study, four kinds of materials were successfully synthesized by different combinations of benzoic acid and chloroform. These synthesized materials were characterized by X-ray powder diffraction (XRD), Fourier-transform infrared spectroscopy (FTIR), scanning electron microscopy (SEM), zeta potential, N_2 adsorption–desorption analysis and thermogravimetric analyses (TGA). Through the adsorption of the target contaminant (CR), a detailed comparison of the adsorption properties of the four materials was performed. The effect of several influential parameters such as adsorbent dosage, solution pH, initial dye concentration, and temperature was well studied and optimized by using batch adsorption study. Moreover, the kinetics, thermodynamics, adsorption properties, and the regeneration performance of the material were researched in detail. The study of the adsorption mechanism aims to expand the application range of MOF materials and seek new effective adsorption materials.

2. Experimental procedure

2.1. Materials

All reagents were purchased from Aladdin Industrial Company (China) and Sigma-Aldrich (US), including zirconium tetrachloride ($ZrCl_4$, 98%), terephthalic acid (H_2BDC, 99%), benzoic acid, chloroform, N, N-dimethylformamide (DMF, 99%), methanol, CR, sodium hydroxide (NaOH, 97%), and hydrochloric acid (HCl, 36.5%). All water used in the synthesis and treatment processes was deionized water.

2.2. Preparation

The acid-promoted and activated UiO-66 (referred to as UiO-66-BA) was prepared by solvating under conventional heating and modified using the reported method [22,23].

2.2.1. Synthesis

A total of 0.386 g (1.67 mmol) of $ZrCl_4$, 0.276 g (1.67 mmol) of H_2BDC, and 6.118 g (50.1 mmol) of benzoic acid were dissolved in DMF (50 mL), and the solution was heated in a Teflon-lined stainless steel autoclave at 393 K for 24 h. Then the autoclave was cooled to room temperature and centrifuged.

2.2.2. Purification

After washed with DMF and methanol three times, the sample obtained by centrifugation was immersed in 100 mL of methanol solution and treated at 373 K for 12 h in the autoclave in order to replace the mother liquor solvent molecules and residual ligands in the pores.

2.2.3. Activation

The synthesized crystals were immersed in chloroform for 5 d so that the synthesized MOF was activated. Then the sample was centrifuged with methanol and finally dried in a vacuum oven at 353 K for 12 h. For comparison, the synthesis of the acid-promoted UiO-66 (referred to as UiO-66-B) did not require an activation step; the activated UiO-66 (referred to as UiO-66-A) was prepared without adding benzoic acid; UiO-66 was ready without the addition of benzoic acid and activation.

2.3. Characterization

XRD pattern was recorded on a Rigaku D/MAX-2500PC diffractometer (Rigaku Co., Japan) using Cu $K\alpha_1$ radiation (λ = 0.15406 nm) operated at 40 kV and 100 mA. FTIR spectra were taken with a Spectrum One FTIR spectrophotometer (Perkin-Elmer, USA) at room temperature. SEM (Model JSM-6360LA, Rigaku Co., Japan) was operated at 30 kV. N_2 adsorption–desorption analysis was performed at 77 K on a porosimetry system ASAP2020 (Micromeritics, USA). Each sample was degassed at 120°C for 120 min prior to analysis. The surface area was estimated using the Brunauer–Emmett–Teller method (S_{BET}), and the pore size distribution was determined by the Barrett-Joyner-Halenda model. TGA of synthesized materials and precursors was obtained by

using a Q50 TGA instrument at a heating rate of 10°C·min^{-1} from 30°C to 800°C in the presence of nitrogen. Zeta potentials were measured by the ZETASIZER Nano-ZSP (Malvern, Britain) with the liquid concentration of 0.75 mg/mL. The pH values were detected by pH meter (PHS-3G, Shanghai REX Scientific Instrument Co., Ltd., Shanghai, China).

2.4. Adsorption–desorption experiments

2.4.1. Adsorption experiments

Accurately weighed 0.1 g/L adsorbent was added to various initial concentrations (50–200 ppm) of CR dye at different pH, and the mixture was stabilized in a water bath for 180 min at 298, 308, and 318 K, respectively. Then the solution was centrifuged at 8,000 rpm for 5 min. The absorbance of CR was measured at a maximum wavelength of 498 nm using a UV spectrophotometer (2550, Shimadzu, Japan) and the equilibrium adsorption capacity was calculated as follows:

$$q_e = \frac{(C_0 - C_e)V}{m} \quad (1)$$

After determination of concentration of dyes vs. time, the dye removal percentage was calculated by Eq. (2):

$$R\% = \frac{(C_0 - C_t)}{C_0} \times 100\% \quad (2)$$

where C_0 (mg/L) and C_e (mg/L) are the initial and equilibrium concentrations of CR solution, respectively; C_t (mg/L) is the concentration of dyes vs. time; V (L) is the volume of the CR solution; and m (g) is the mass of adsorbent.

2.4.2. Desorption experiments

The feasibility of the reproduction of adsorbed saturated materials was evaluated by using solvent desorption techniques. The solution of DMF was used as an eluent to regenerate a series of UiO-66 materials. The used UiO-66 materials were added to the DMF, and the mixture was sonicated for 30 min and dried in an oven at 373 K. Finally, the regenerated adsorbents were used to adsorb CR again.

3. Results and discussion

3.1. Characterization

X-ray diffraction patterns of samples were characterized and shown in Fig. 1(a). UiO-66 model is consistent with the reported in the literature [24,25], indicating the successful synthesis. It can be seen that a very broad peak (spanning a 2θ range of 2°–7°) is observed in the powder X-ray diffraction patterns of UiO-66-B. We unambiguously assign this "broad peak" to very tiny "nanoregions" of missing cluster defects promoted by monocarboxylic acid modulation [26,27]. However, this "broad peak" is not seen on the patterns of UiO-66-BA. This phenomenon may be due to activation process which can reduce unreacted benzene dicarboxylic acid linkers into its structure to get defect-free structure [21]. In addition, according to the intensity of the diffraction peak, the addition of benzoic acid promotes the form of high crystallinity UiO-66.

To further understand the surface characteristics of materials, FTIR spectra were characterized to show the coordination of organic linkers and metal units, as shown in Fig. 1(b). For UiO-66, the absorption peaks at wavenumbers of 3,423 cm^{-1}, 1,574 cm^{-1} (1,401 cm^{-1}), and 1,506 cm^{-1} represent O–H group at the external surface, the asymmetric stretching of O–C–O in the BDC ligand, and the typical vibration present in a C=C of benzene ring, respectively [28]. In addition, the peaks at 664 and 748 cm^{-1} are attributed to μ^3–O stretching with Zr–(OC) [14]. These peaks on UiO-66 appear on the other three materials, indicating the similarity of these materials to UiO-66. However, there is a noteworthy place that a weak peak at wavenumber of 1,708 cm^{-1} representing the stretching vibrations of C=O in benzoic appears on UiO-66-B and UiO-66-BA. This may be due to the addition of benzoic acid.

Meanwhile, the morphology and structure of these materials were showed by SEM in Fig. 2. As shown in Figs. 2(a) and (b), samples UiO-66 and UiO-66-A show an aggregated structure composed of nanocrystals due to the continuous secondary nucleation of UiO-66 nuclei [29]. However, the crystallinity of UiO-66-A is more regular than that of UiO-66,

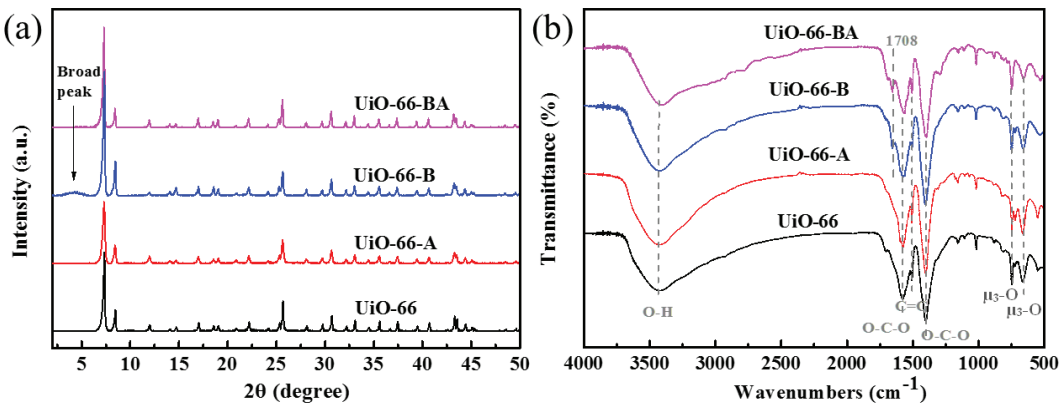

Fig. 1. (a) XRD patterns and (b) FTIR spectra of materials.

showing a more cubic structure, probably due to the activation effect of chloroform. In the crystallization synthesis of UiO-66-B and UiO-66-BA, a competitive coordinator of the ($ZrCl_4$) metal cluster is produced between H_2BDC and a regulator (benzoic acid) with same carboxyl group, breaking down the original coordination between the ligand with the metal clusters. Therefore, the nucleation of UiO-66-B is inhibited, resulting in the rate of decline and the nucleated small grains can grow into larger grains [30,31]. In addition, due to the addition of the acid, some zirconium clusters tend to combine with benzoic acid or exchange between benzoic acid and linker molecules at the coordination sites, which limit the secondary nucleation and form a non-agglomerated crystal structure [32], as shown in Figs. 2(c) and (d). However, as compared with UiO-66-B, UiO-66-BA produced an almost perfect structure of UiO-66, angular rudiment of octahedrons shown in Fig. 2(d), confirming the defect-free structure of UiO-66-BA.

The same, the porosities and surface areas of all samples were measured by nitrogen adsorption at 77 K (Fig. 3).

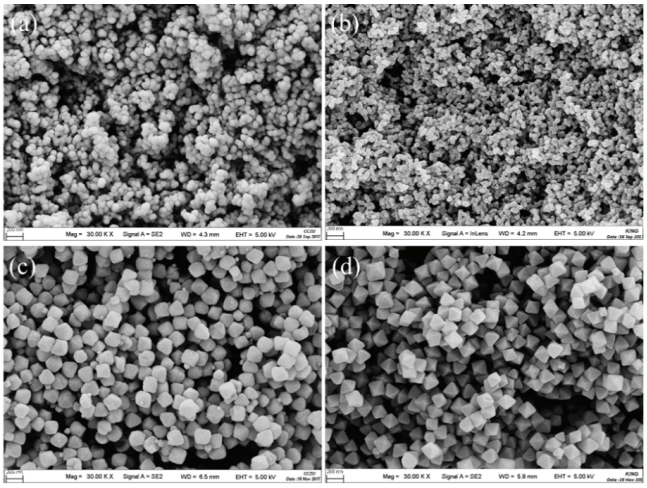

Fig. 2. (a) SEM images of UiO-66, (b) UiO-66-A, (c) UiO-66-B, and (d) UiO-66-BA.

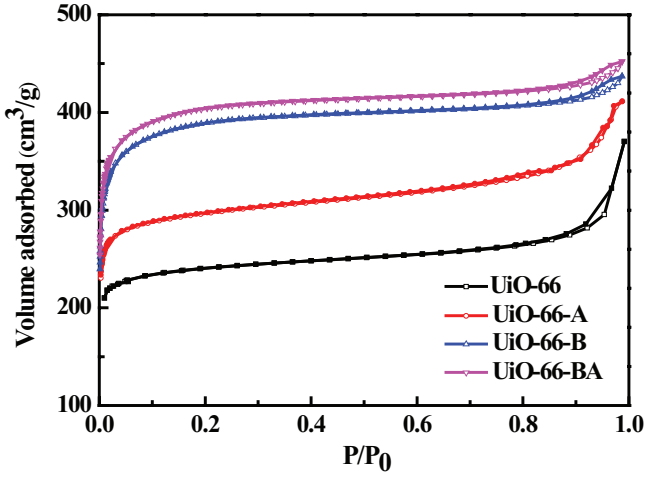

Fig. 3. N_2 adsorption/desorption of the UiO-66, UiO-66-A, UiO-66-B, and UiO-66-BA.

The details of textural properties were given in Table 1. As evidenced by reversible Type-I N_2 adsorption isotherms, all of them exhibit permanent microporosity. The surface area of UiO-66 sample is 750 m^2/g, which is similar to some of the reported results [33,34]. However, after activation with chloroform, the absence of unreacted BDC may help to obtain a more perfectly structured UiO-66, increasing the specific surface area and pore size [14,35]. In addition, the specific surface area and pore size of UiO-66 were increased with the addition of benzoic acid and changed with the acid concentration because of their enhanced crystallinity, consistent with previous reports [16,20].

To examine the effect of acid regulation and chloroform activation on the thermal stability of UiO-66, the TGA patterns with derivative curve were shown in Fig. 4. From the in-house derivative curves, it can be seen that the thermal weight loss of four materials can be divided into three stages: surface water evaporation (<120°C), decomposition of guest molecules (150°C–480°C), and collapse of structure (480°C–610°C). The weight loss of UiO-66 and its derivative nanocrystals occur essentially at the same temperature, indicating that the thermal stability of the backbone is not affected by the addition and activation of acids [36]. The weight loss of UiO-66-A is smaller than that of UiO-66 in the second stage, and it is understood that the reduction of residual ligand and DMF in the pore is due to activation. At the same time, the greater thermal weight loss on UiO-66-B may be due to the remaining benzoic acid molecules in the pore size.

Table 1
Parameters of porous structure for the samples

Sample	S_{BET} (m^2/g)	V_{total} (cm^3/g)	V_{micro} (cm^3/g)	V_{meso} (cm^3/g)	P_{diam} (nm)
UiO-66	750	0.448	0.316	0.132	2.43
UiO-66-A	905	0.531	0.329	0.202	2.51
UiO-66-B	1,186	0.672	0.457	0.215	2.96
UiO-66-BA	1,230	0.699	0.462	0.237	3.02

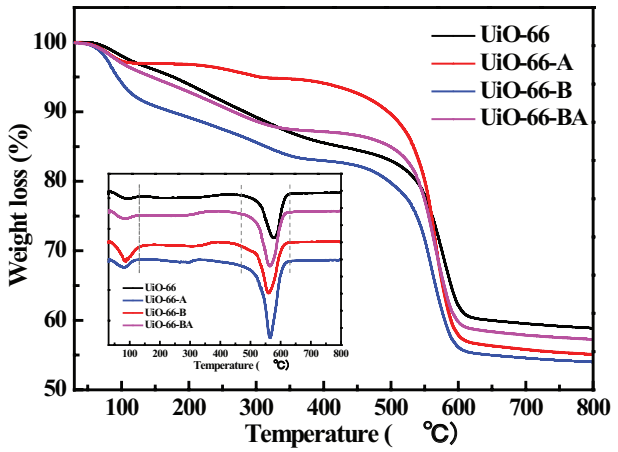

Fig. 4. TGA curves of UiO-66, UiO-66-A, UiO-66-B, and UiO-66-BA and their derivative curves inside.

3.2. Effect of operational parameters on dye removal

3.2.1. Effect of adsorbent dosage

A series of batch experiments were carried out by adding different amount of adsorbent to 50 mL of CR solution (initial dye concentration of 50 mg/L), and the mixture was oscillated at 298 K and pH = 7 for 180 min. Fig. 5 shows the effect of adsorbent dosage on CR adsorption. As can be seen from the figure, with the increase of adsorbents doses, there are different degrees of decrease in the amount of CR adsorbed for all four adsorbents, while the dye removal efficiency increases significantly. In fact, the decreased adsorption capacity can be attributed to an increase in the unused active site on the adsorbent, resulting in a decrease in adsorption capacity per unit mass of adsorbent [37]. The higher removal efficiency is due to the enhancement in the available adsorptive surface area and active surface sites [38]. As can be observed, UiO-66 and UiO-66-A have significantly less adsorption capacity and removal efficiency than the other two materials because their crystals have a low adsorption area (as BET analysis confirmed) and active sites due to the lack of acid regulation. Also, UiO-66-B has a slightly lower adsorption efficiency in comparison with UiO-66-BA because non-activated UiO-66-B shows a relatively missing crystal structure, making them hydrophilic [39]. This hydrophilicity promotes the interaction of UiO-66 with water molecules instead of adsorbates, thus resulting in a decreased adsorption capacity.

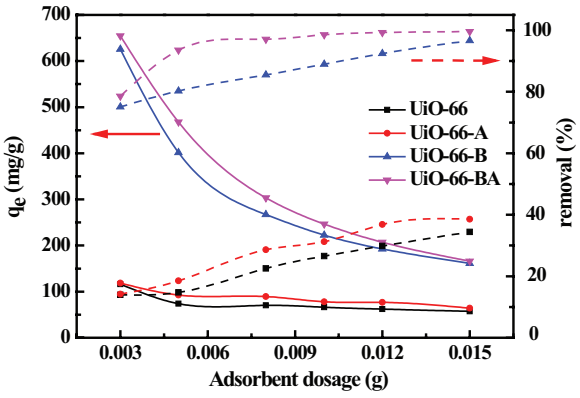

Fig. 5. Effect of UiO-66, UiO-66-A, UiO-66-B, and UiO-66-BA dosage on sorption of CR.

3.2.2. Effect of pH

The study of initial solution pH and zeta potential of adsorbents can provide important information for the effect of protonation and deprotonation of adsorbents on the CR adsorption and the study of adsorption mechanism. The mixture containing 5 mg of adsorbent in 50 mL of CR solution (initial dye concentration of 50 mg/L) was shaken in a water bath at 298 K for 180 min. The pH in this study was adjusted with 0.1 mol NaOH and 0.1 mol HCl and varied in the range of 3–11. The amount of adsorption and the zeta potential distribution of the adsorbents at different pH were shown in Figs. 6(a) and (b), respectively. In this study, CR is an amphoteric adsorbate that can be present as CR^+ or CR^- depending on the pH of the solution. The pKa value of CR is 5.5 [40], which suggests that CR mainly exists in an anionic form at pH > 5.5 and acidic or neutral at pH < 5.5, as shown in Fig. 7. As shown in Fig. 6(a), the equilibrium adsorption capacity remained stable without significant loss when the pH decreased from 7 to 3. The four materials exhibited the highest adsorption capacity at pH = 7. The adsorption capacity of UiO-66-B and UiO-66-BA is about 4–4.8 times that of the other two materials. The only slight decrease of the adsorption capacity at pH = 3 may be attributed to electrostatic repulsion between CR in the form of cationic due to protonation and

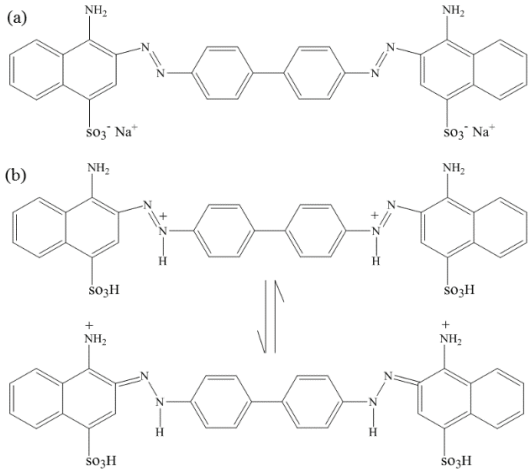

Fig. 7. Structure of CR at (a) pH > 5.5 and (b) pH < 5.5.

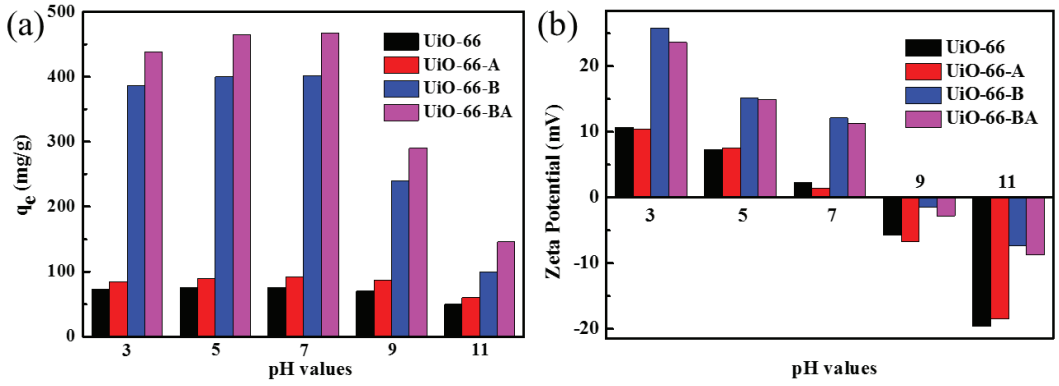

Fig. 6. (a) Effect of solution pH on the adsorption of CR over adsorbents and (b) zeta potential of adsorbents at different pH values.

enhanced positively charged adsorbents under strong acid conditions. The same, in the alkali environments (pH = 9 and 11), the lower adsorption at higher pH may be on account of the abundance of OH^-, and the ionic repulsion between the negative charge on the surface of adsorbents and negative ionic organic compounds [41,42]. The acid-promoted UiO-66 has more positive charge and can have a stronger electrostatic interaction with the anionic dye (CR), which is an important reason that the adsorbed amount of CR by UiO-66-B and UiO-66-BA can be much larger for UiO-66 and UiO-66-A.

3.2.3. Effect of concentration and temperature on adsorption

The effect of concentration and temperature on adsorption was investigated by adding 5 mg of adsorbent to 50 mL of different concentrations of CR solution and shaking at different temperatures and pH = 7 for 180 min. Fig. 8(a) shows the effect of initial concentration of CR on the adsorption capacity of four kinds of materials. With the increase of CR concentration from 50 to 200 mg/L, the adsorption capacity of UiO-66-B and UiO-66-BA to CR increased rapidly, while the adsorption capacity of UiO-66-A increased gently. Because of the low concentration, the adsorption cannot reach saturation. With the increase of concentration, the increasing number of collisions between the dye ions and adsorbents, due to higher initial dye concentration, brings higher driving force of the concentration gradient, and the greater impetus can be provided to overcome the mass transfer resistance of CR from the liquid phase to the adsorbent surface, so the adsorption capacity becomes larger [43]. When the adsorption reaches equilibrium, the adsorption capacity tends to be constant. However, the adsorption capacity of UiO-66 is similar with the increase of CR concentration, probably because CR adsorption on UiO-66 has approached an equilibrium state of adsorption at about 50 mg/L. Meanwhile, Fig. 8 displays the effect of temperature on the adsorption of four materials in different concentrations of solution. It can be seen that the equilibrium adsorption capacity on four materials increases with temperature for the different initial concentrations of CR at 298–318 K, indicating that the adsorption reaction is endothermic, and the elevated temperature is favorable for the adsorption. The temperature rises accelerate the molecular thermal motion, thereby increasing the physical adsorption rate for CR. In addition, the increase in temperature provides more energy for the reaction process and promotes the formation of stable chemical bonds between the surface of the adsorbent and the organic matter, thus improving the adsorption effect [44].

3.2.4. Effect of time on adsorption

Meanwhile, the adsorption performance will change greatly with the change of contact time. Fig. 9 showed the effect of contact time by adding 5 mg of adsorbent to 50 mL of CR solution (initial dye concentration of 50 mg/L) and being oscillated at 298 K and pH = 7. It could be seen that the adsorption rates of UiO-66-BA and UiO-66-B were very fast in the initial 30 min, and the removal rates of CR were 81.1% and 69.1%, respectively, while that of UiO-66 and UiO-66-A were much lower, and the removal rates of CR were only 11.5% and 12.8%, respectively. After 120 min, the adsorption curve hardly changed, and the adsorption reached equilibrium in 180 min. The adsorption rate of CR on UiO-66-BA reached 93.6% for CR, while that of UiO-66 had only 15.4%. It could be seen that the benzoic acid-regulated and chloroform-activated UiO-66 had greatly enhanced the adsorption performance to CR. From the mechanism of mass transfer, at the initial stage of adsorption, the adsorption rate of CR on UiO-66-BA increased rapidly with the prolongation of adsorption time. At this time, the adsorption of CR may mainly occur on the surface of UiO-66-BA and the outer surface of the pores. At the later stage of adsorption, the adsorption was controlled by diffusion, which may occur on the inner surface of the channel, so the adsorption rate is slowed down. After 180 min, the adsorption reached an equilibrium stage. Fig. 9 shows the decolorization of the CR solution after dosing the corresponding adsorbent.

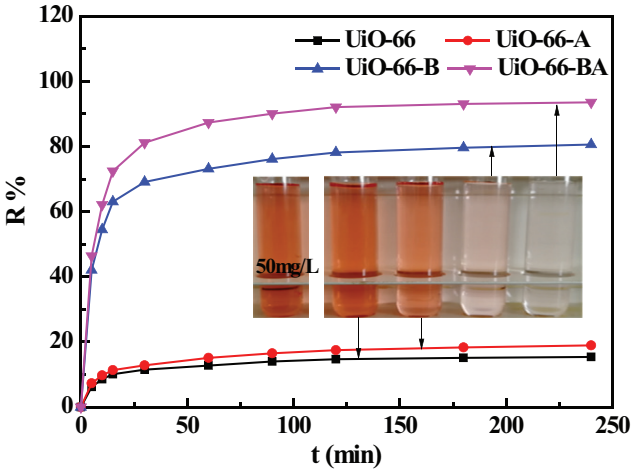

Fig. 9. Effect of adsorption time on the adsorption performance of four materials.

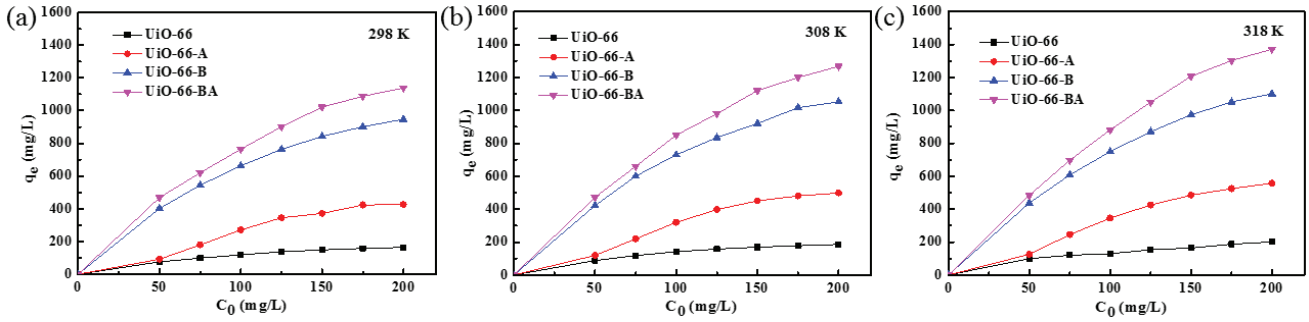

Fig. 8. Effects of concentration on the CR adsorption capacity for four materials at (a) 298 K, (b) 308 K, and (c) 318 K.

3.3. Adsorption kinetic

The study on adsorption kinetics is helpful to determine the mechanism of adsorption and to study the efficiency of adsorbents to remove contaminants [45,46]. In order to find the potential rate control step for adsorbing CR on adsorbents, we chose the pseudo-first-order model [47], the pseudo-second-order kinetics model [48], the intraparticle diffusion model [49], and the Elovich model [50] to fit the experimental data.

The pseudo-first-order model is written as follows:

$$\ln\left(q_e - q_t\right) = \ln q_e - k_1 \cdot t \tag{3}$$

The pseudo-second-order model is written as follows:

$$t \cdot q_t^{-1} = k_2^{-1} \cdot q_e^{-2} + t \cdot q_e^{-1} \tag{4}$$

The intraparticle diffusion equation can be described as follows:

$$q_t = k_i \cdot t^{1/2} + C \tag{5}$$

The Elovich equation is another kinetic model equation based on the adsorption capacity expressed as follows:

$$q_t = \beta \ln\left(\alpha\beta\right) + \beta \ln t \tag{6}$$

where q_e and q_t (mg/g) are the adsorption capacity at equilibrium and at any time t (min), respectively. k_1 (min^{-1}) and k_2 (g·mg^{-1}·min^{-1}) are the rate constants of the first-order adsorption and the second-order adsorption. The plot of ln (q_e–q_t) vs. t is used to obtain pseudo-first-order parameters q_e and k_1, and that of t/q_t vs. t is employed to deduce pseudo-second-order parameters k_2 and q_e. k_i (mg·g^{-1}·min$^{-1/2}$) and C are the intraparticle diffusion rate constant and the intercept, which can be assessed from the slope of the linear plot of q_t *vs.* $t^{1/2}$. α and β are the Elovich constant that represent the initial adsorption rate (g·mg^{-1}·min^{-1}) and the desorption constant (g·mg^{-1}·min^{-1}), respectively. The Elovich constants could be obtained from the graphs of q_t vs. ln t.

Adsorption kinetics studies were performed by shaking 50 mL of different concentrations of CR solution containing 5 mg of adsorbent at 298 K and pH = 7. The correlation coefficient of each kinetic equation was calculated and rendered in Table 2. The results showed that the pseudo-second-order model could better explain the adsorption processes on these four materials because this model exhibited the linear plot with the higher value of correlation coefficients (R^2, 0.987–0.997) for all adsorbents and the calculated q_e value of the pseudo-second-order model was also closed to the experimental data. Moreover, the intraparticle diffusion showed better concordance than the pseudo-first-order model, but the R^2 value of this model was lower than the second-order kinetic. The comparison of equilibrium rate constants (k_2) indicated that the UiO-66-B removed dyes swifter than UiO-66-BA. Moreover, the decrease in k_2 value with increasing dye concentration suggested that the increase of concentration would decrease the initial adsorption rate.

Table 2
Correlation coefficient of kinetic equations for the CR adsorption

Adsorbent type	Dye concentration	$q_{e,exp}$	Quasi-first order			Quasi-second order			Intraparticle diffusion			Elovich		
			K_1	q_e	R^2	K_2	q_e	R^2	k_i	C	R^2	α	β	R^2
UiO-66	50	76.82	0.02025	41.29	0.989	1.25×10^{-3}	79.74	0.996	2.96	41.09	0.987	0.327	11.70	0.977
	125	137.38	0.02006	91.72	0.990	6.73×10^{-4}	144.72	0.997	7.15	51.77	0.991	0.069	23.69	0.989
	200	164.78	0.01956	99.27	0.983	4.41×10^{-4}	172.12	0.992	7.39	74.75	0.986	0.065	28.11	0.979
UiO-66-A	50	94.74	0.02395	52.68	0.991	7.73×10^{-3}	98.43	0.994	4.24	41.67	0.992	0.168	15.03	0.995
	125	345.74	0.01813	222.15	0.981	8.01×10^{-4}	367.65	0.994	15.92	151.43	0.978	0.015	67.75	0.978
	200	426.35	0.01555	235.75	0.952	2.01×10^{-4}	448.43	0.992	17.13	236.32	0.955	0.020	77.79	0.938
UiO-66-B	50	403.05	0.01946	138.39	0.959	4.32×10^{-3}	409.84	0.990	8.32	300.56	0.989	0.778	46.43	0.918
	125	763.25	0.01898	488.59	0.985	1.01×10^{-4}	877.19	0.992	33.17	350.98	0.986	0.014	143.17	0.961
	200	946.93	0.01718	568.11	0.989	7.04×10^{-5}	990.09	0.987	44.07	399.09	0.974	0.011	159.96	0.991
UiO-66-BA	50	467.83	0.02475	172.39	0.969	3.91×10^{-3}	478.47	0.995	9.95	354.43	0.985	0.384	57.91	0.898
	125	901.71	0.02141	562.60	0.982	8.35×10^{-5}	943.39	0.991	40.38	422.62	0.987	0.012	155.00	0.981
	200	1,138.78	0.01624	671.22	0.984	5.74×10^{-5}	1,190.48	0.988	48.64	516.90	0.986	0.008	195.22	0.989

3.4. Adsorption isotherms

Adsorption isotherms can provide information about the surface properties, sorption mechanism, and the affinity of adsorbents. In this study, adsorption isotherms models such as Langmuir, Freundlich, Temkin, and Dubinin–Radushkevich (D–R) were used to describe the relationship between the adsorbed amount of CR and its equilibrium concentration. Jin et al. [51] assume that there is no interaction between adsorbate molecules, and the adsorption is at homogeneous sites on the adsorbent surface. The dye molecules occupy a site where no adsorption takes place again. Another important parameter R_L, the separation factor or equilibrium parameter, is used to judge if an adsorption system is "favorable" or "unfavorable" [52]. The Langmuir isotherm equations and the separation factor are described as follows:

$$C_e \cdot q_e^{-1} = q_0^{-1} \cdot k_L^{-1} + C_e \cdot q_0^{-1} \tag{7}$$

$$R_L = \frac{1}{1 + K_L \cdot C_0} \tag{8}$$

where C_e (mg·L^{-1}) and q_e (mg·g^{-1}) represent the equilibrium concentration and the amount of adsorbate at equilibrium, respectively. q_0 (mg·g^{-1}) and C_0 (mg·L^{-1}) signify the Langmuir constant concerned with the theoretical maximum adsorption quantity and the initial concentration, respectively. k_L is Langmuir constant. For $R_L > 1$, the adsorption is unfavorable; for $R_L = 1$, linear; for $0 < R_L < 1$, favorable; and for $R_L = 0$, irreversible. k_F and $1/n$ represent the Freundlich constant and heterogeneity factor, respectively.

The Freundlich isotherm model makes a proposal that considers a monolayer sorption with a heterogeneous positive distribution of active sites and deems that there exist interactions between adsorbed species [53]. This model can be expressed by the following equation:

$$\ln q_e = \frac{1}{n} \ln C_e + \ln k_F \tag{9}$$

where k_F and $1/n$ represent the Freundlich constant and heterogeneity factor, respectively. The value of n indicates the favorability of adsorption. If $n > 1$, the nature of adsorption is favorable.

The Temkin isotherm model presumes that the adsorption heat decreases linearly with increasing the coverage of absorbent surface [54]. Uniform distribution of the binding energy is one of the features in this model. The linear form of this isotherm is described as follows:

$$q_e = B \ln K_T + B \ln C_e \tag{10}$$

where B is an adsorption constant characterizing the free energy of adsorption and K_T is the equilibrium binding constant related to the maximum binding energy (L·g^{-1}).

The D–R [55] isotherm is an empirical model which assumes that adsorption can take place as the multilayer adsorption. Generally, this isotherm is utilized to describe the adsorption mechanism with the distribution of Gaussian energy onto a heterogeneous surface. The linear equation of D–R model can be represented as follows:

$$\ln q_e = \ln q_d - \beta \varepsilon^2 \tag{11}$$

$$\varepsilon = RT \ln\left(1 + \frac{1}{C_e}\right) \tag{12}$$

$$E = \frac{1}{\sqrt{2\beta}} \tag{13}$$

where q_d is the theoretical adsorption capacity (mg·g^{-1}), ε represents Polanyi potential and β shows the D–R isotherm constant. R is the gas constant (8.314 J·mol^{-1}·K^{-1}), and T is the absolute temperature (K). TE (kJ·mol^{-1}) indicates that the sorption is physical or chemical. If $E < 8$ kJ·mol^{-1}, the adsorption process was naturally physical. If its amount was between 8 and 16 kJ·mol^{-1}, it was chemical in nature.

Adsorption isotherms studies were performed by shaking 50 mL of CR solution (initial dye concentration of 50 mg/L) containing 5 mg of adsorbent at 298 K, pH = 7. The constant parameters of adsorption isotherm equations and the correlation coefficient (R^2) for each model are presented in Table 3. Because R^2 values of the Langmuir equation are higher than other isotherms equations, the Langmuir model can be more suitable for experimental data. $0 < R_L < 1$ means that the adsorption system is favorable. Therefore, this result indicated that the adsorptions of CR were monolayer uniform adsorptions. It is noteworthy that the adsorption of UiO-66-A to CR is better matched to the D–R model due to the higher R^2 value (0.990), confirming the multilayer adsorption and heterogeneous surface of this nanocomposite. In the meantime, the value of n for Freundlich isotherm is 0.89 for UiO-66-A, which represents the adverse property of adsorption. In addition, the results of D–R isotherm model indicate

Table 3
Linearized isotherm coefficients for CR adsorption at different concentrations

Adsorbent type	Langmuir				Freundlich			Temkin			Dubinin–Radushkevich		
	q_0	K_L	R_L	R^2	k_F	n	R^2	B	K_T	R^2	q_d	E	R^2
UiO-66	259.74	0.009	0.341	0.995	10.38	1.86	0.984	62.63	0.077	0.974	171.74	0.035	0.972
UiO-66-A	694.44	0.012	0.327	0.982	1.88	0.89	0.885	261.02	0.037	0.966	498.63	0.030	0.990
UiO-66-B	1124.85	0.047	0.096	0.996	178.29	2.73	0.991	236.49	0.519	0.989	895.47	0.113	0.875
UiO-66-BA	1270.65	0.085	0.055	0.987	319.68	3.47	0.977	216.86	1.958	0.938	1,051.61	0.172	0.815

the adsorption process as physical in nature (E < 8 kJ·mol^{-1}) for all prepared adsorbents.

In order to better illustrate the CR adsorption capacity of Zr-based MOFs synthesized in this paper, Table 4 lists the maximum adsorption capacity of CR for various MOFs reported in recent years. From the table, the adsorption capacity of Zr-based MOFs to CR in water exceeds that of many metal-based MOFs, except Ni-based MOFs, and is much larger than that of commercial activated carbon, suggesting that the acid-promoted and activated Zr-based MOFs are suitable as an adsorbent for the removal of CR dye in wastewater.

3.5. Thermodynamic analysis

To study the intrinsic energy changes during the adsorption process, the thermodynamic parameters referred to the change in the Gibbs free energy (ΔG), enthalpy (ΔH), and entropy (ΔS) are investigated and calculated from the following equations:

$$K_c = \frac{q_e}{C_e} \tag{14}$$

$$\Delta G = -RT \ln K_c \tag{15}$$

$$\ln K_c = -\frac{\Delta H}{RT} + \frac{\Delta S}{R} \tag{16}$$

where q_e (mg·g^{-1}), C_e (mg·L^{-1}), R (8.314.1914 J·mol^{-1}·K^{-1}), T (K), and K_c (mg·g^{-1}) are the amount of CR absorbed per unit mass of CR, the equilibrium concentration, the universal gas constant, temperature, and the Freundlich constant, respectively.

Thermodynamic studies were performed at different temperatures and pH = 7 for 180 min by adding 5 mg of adsorbent to 50 mL of CR solution (initial dye concentration of 50 mg/L). The thermodynamic parameters at various temperatures are shown in Table 5. The negative values of ΔG at different temperatures and the positive value of ΔH mean that the CR adsorption is spontaneous and endothermic reaction [62]. Meanwhile, ΔH (<40 kJ·mol^{-1}) also indicates that the adsorption of CR onto four adsorbents may be physical processes, based on the opinion of Kara et al. [63] that the ΔH of chemical adsorption is more than 40 kJ·mol^{-1}. Moreover, the decreasing value of ΔG with rising temperature implies that the CR adsorption on these adsorbents is more spontaneous at higher temperature. The positive values of ΔS indicate that the randomness of the adsorption process increases because the number of desorbing water molecules is greater than the number of adsorbed CR molecules (more water molecules can be desorbed by adsorbing CR molecules because CR molecules are larger than water molecules).

Table 4
Comparison of the CR adsorption capacity of prepared adsorbents with the reported similar materials

Adsorbent	q_{max} (mg/g)	Reference
UiO-66-B	1,100.18	This study
UiO-66-BA	1,371.91	This study
Bi-FMOF	72	[56]
MIL-68(In) microrods	318	[57]
Terbium luminescent MOFs	637	[58]
3D copper(II) MOFs	656	[59]
Ni/Cu mixed-component MOFs	1,100	[60]
MIL-68(In) nanorods	1,204	[57]
Ni-MOFs	2,046	[61]
Activated carbon	300	[40]

FMOF – fluorous metal-organic framework.

3.6. Regeneration

The regeneration of the adsorbent is critical in practical adsorption applications. 5 mg of adsorbent was added to 50 mL of CR solution with concentration of 50 mg/L under the stirrer at pH = 7 for 180 min. Fig. 10 shows that the regenerated UiO-66-B and UiO-66-BA is reusable because

Table 5
Thermodynamic equilibrium constant K and relative thermodynamic parameters

Adsorbent	T (K)	K_c (mL·g^{-1})	ΔG (kJ·mol^{-1})	ΔH (kJ·mol^{-1})	ΔS (J·mol^{-1}·K^{-1})
UiO-66	298	1.79	–1.45	12.64	0.047
	308	2.12	–1.92		
	318	2.47	–2.34		
UiO-66-A	298	2.26	–2.02	15.67	0.060
	308	3.12	–2.91		
	318	3.35	–3.21		
UiO-66-B	298	40.85	–9.19	20.92	0.101
	308	53.84	–10.25		
	318	67.57	–11.21		
UiO-66-BA	298	145.28	–12.32	28.43	0.136
	308	166.07	–13.09		
	318	300.56	–15.04		

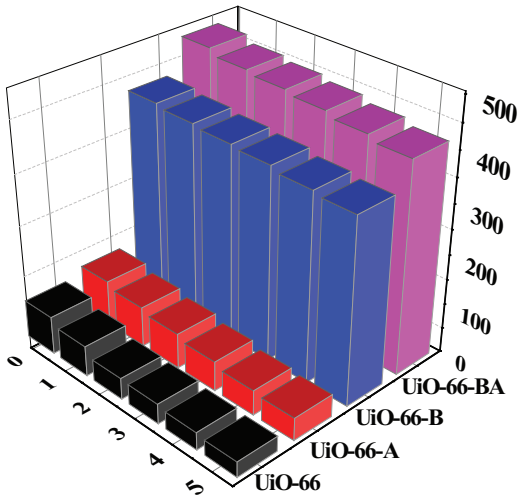

Fig. 10. Recycling of prepared adsorbents for CR adsorption.

of the stable adsorption capacity during the four adsorption process. After five cycles, the adsorption rates decreased by only 9.5 % and 6.4 %, respectively, indicating that it is effective to regenerate UiO-66-B and UiO-66-BA with DMF as the analytical solvent. However, the regeneration of UiO-66 and UiO-66-A materials is not satisfactory.

4. Conclusions

Acid-promoted and activated UiO-66 was successfully synthesized by a simple solvothermal method. Characterization results showed that the addition of benzoic acid and chloroform activation can control the crystal structure, the size of the specific surface area, and pore size. Meanwhile, the addition of acid can provide more positive charge on the surface of materials, and a more perfect crystal structure can be manufactured by chloroform activation. A series of experiments showed that the maximum adsorption amount of UiO-66-B and UiO-66-BA to CR reached 1,100 and 1371 $mg \cdot g^{-1}$, respectively, which was five to seven times that of UiO-66. Enhanced positive potential, larger adsorption area and active site, and better hydrophobic properties may explain the reason for the increased adsorption. Meanwhile, the results confirmed that the adsorption process could be well fitted by Langmuir isotherm and the pseudo-second-order kinetics, respectively, indicating that the adsorption of CR was monolayer uniform adsorption. In addition, thermodynamic studies showed that the adsorption of CR was a spontaneous endothermic reaction and physical process. The large amount of CR adsorption and the convenient and efficient regenerative properties suggested that UiO-66-B and UiO-66-BA can be used as a promising adsorbent in the adsorptive removal of CR dyes. In short, this study highlights the importance of precision MOFs material synthesis in adsorption process.

Acknowledgment

The authors sincerely acknowledge the financial supports from the National Natural Science Foundation of China (Nos. 41371446 and 41271498).

References

[1] M. Liu, J. Xu, B. Cheng, W. Ho, J. Yu, Synthesis and adsorption performance of $Mg(OH)_2$ hexagonal nanosheet–graphene oxide composites, Appl. Surf. Sci., 332 (2015) 121–129.
[2] X. Liu, W. Gong, J. Luo, C. Zou, Y. Yang, S. Yang, Selective adsorption of cationic dyes from aqueous solution by polyoxometalate-based metal–organic framework composite, Appl. Surf. Sci., 362 (2016) 517–524.
[3] X. Yuan, C. Zhou, Y. Jin, Q. Jing, Y. Yang, X. Shen, Q. Tang, Y. Mu, A.K. Du, Facile synthesis of 3D porous thermally exfoliated g-C_3N_4 nanosheet with enhanced photocatalytic degradation of organic dye, J. Colloid Interface Sci., 468 (2016) 211–219.
[4] Y.J. Tan, L.J. Sun, B.T. Li, X.H. Zhao, T. Yu, N. Ikuno, K. Ishii, H.Y. Hu, Fouling characteristics and fouling control of reverse osmosis membranes for desalination of dyeing wastewater with high chemical oxygen demand, Desalination, 419 (2017) 1–7.
[5] J. Guo, S. Chen, L. Liu, B. Li, P. Yang, L. Zhang, Y. Feng, Adsorption of dye from wastewater using chitosan–CTAB modified bentonites, J. Colloid Interface Sci., 382 (2012) 61–66.
[6] C.F. Wang, E.M. Mäkilä, C. Bonduelle, J. Rytkönen, J. Raula, S. Almeida, A. Närvänen, J.J. Salonen, S. Lecommandoux, J.T. Hirvonen, Functionalization of alkyne-terminated thermally hydrocarbonized porous silicon nanoparticles with targeting peptides and antifouling polymers: effect on the human plasma protein adsorption, ACS Appl. Mater. Interfaces, 7 (2015) 2006–2015.
[7] M.Z. Momčilović, M.S. Ranđelović, M.M. Purenović, J.S. Đorđević, A. Onjia, B. Matović, Morpho-structural, adsorption and electrochemical characteristics of serpentinite, Sep. Purif. Technol., 163 (2016) 72–78.
[8] B. Acevedo, R.P. Rocha, M.F.R. Pereira, J.L. Figueiredo, C. Barriocanal, Adsorption of dyes by ACs prepared from waste tyre reinforcing fibre. Effect of texture, surface chemistry and pH, J. Colloid Interface Sci., 459 (2015) 189–198.
[9] H. Cai, J. Zhou, S. Kitagawa, Metal–organic frameworks (MOFs), Chem. Soc. Rev., 43 (2014) 5415–5418.
[10] G.P. Yang, L. Hou, X.J. Luan, B. Wu, Y.Y. Wang, Molecular braids in metal–organic frameworks, Chem. Soc. Rev., 41 (2012) 6992–7000.
[11] J.M. Hu, V.A. Blatov, B. Yu, H.K. Van, G.H. Cui, An unprecedented "strongly" self-catenated MOF containing inclined catenated honeycomb-like units, Dalton Trans., 45 (2016) 2426–2429.
[12] S.Y. Hao, S.-X. Hou, K.V. Hecke, G.-H. Cui, Construction of noninterpenetrating and interpenetrating Co(II) networks with halogenated carboxylate modulated by auxiliary N-donor co-ligands: structural diversity, electrochemical and photocatalytic properties, Dalton Trans., 46 (2017) 1951–1964.
[13] J.-W. Cui, S.-X. Hou, K.V. Hecke, G.-H. Cui, Rigid versus semi-rigid bis(imidazole) ligands in the assembly of two Co(II) coordination polymers: structural variability, electrochemical properties and photocatalytic behavior, Dalton Trans., 46 (2017) 2892–2903.
[14] L. Valenzano, B. Civalleri, S. Chavan, S. Bordiga, M.H. Nilsen, S. Jakobsen, K.P. Lillerud, C. Lamberti, Disclosing the complex structure of UiO-66 metal organic framework: a synergic combination of experiment and theory, Chem. Mater., 23 (2011) 1700–1718.
[15] Z. Hasan, D.W. Cho, I.H. Nam, C.M. Chon, H. Song, Preparation of calcined zirconia-carbon composite from metal organic frameworks and its application to adsorption of crystal violet and salicylic acid, Materials, 9 (2016) 261–271.
[16] K. Wang, C. Li, Y. Liang, T. Han, H. Huang, Q. Yang, D. Liu, C. Zhong, Rational construction of defects in a metal–organic framework for highly efficient adsorption and separation of dyes, Chem. Eng. J., 289 (2016) 486–493.
[17] B.J. Yao, W.L. Jiang, Y. Dong, Z.X. Liu, Y.B. Dong, Post-synthetic polymerization of UiO-66-NH_2 nanoparticles and polyurethane oligomer toward stand-alone membranes for dye removal and separation, Chem. Eur. J., 22 (2016) 10565–10571.
[18] Y. Li, Y. Liu, W. Gao, L. Zhang, W. Liu, J. Lu, Z. Wang, Y.J. Deng, Microwave-assisted synthesis of UIO-66 and its adsorption performance towards dyes, CrystEngComm, 16 (2014) 7037–7042.
[19] S. Ling, Dynamic acidity in defective UiO-66, J. Chem. Sci., 7 (2016) 4706–4712.
[20] J. Qiu, Y. Feng, X. Zhang, M. Jia, J. Yao, Acid-promoted synthesis of UiO-66 for highly selective adsorption of anionic dyes: adsorption performance and mechanisms, J. Colloid Interface Sci., 499 (2017) 151–158.
[21] M.R. Azhar, H.R. Abid, V. Periasamy, H. Sun, M.O. Tade, S. Wang, Adsorptive removal of antibiotic sulfonamide by UiO-66 and ZIF-67 for wastewater treatment, J. Colloid Interface Sci., 500 (2017) 88–95.
[22] C. Gomes Silva, I. Luz, F.X. Llabres i Xamena, A. Corma, H. Garcia, Water stable Zr-benzenedicarboxylate metal–organic frameworks as photocatalysts for hydrogen generation, Chem., 16 (2010) 11133–11138.
[23] M. Kandiah, M.H. Nilsen, S. Usseglio, S. Jakobsen, U. Olsbye, M. Tilset, C. Larabi, E.A. Quadrelli, F. Bonino, K.P. Lillerud, Synthesis and stability of tagged UiO-66 Zr-MOFs, Chem. Mater., 22 (2010) 6632–6640.
[24] C.G. Piscopo, A. Polyzoidis, M. Schwarzer, S. Loebbecke, Stability of UiO-66 under acidic treatment: opportunities and limitations for post-synthetic modifications, Microporous Mesoporous Mater., 208 (2015) 30–35.

[25] M.J. Katz, Z.J. Brown, Y.J. Colón, P.W. Siu, K.A. Scheidt, R.Q. Snurr, J.T. Hupp, O.K. Farha, A facile synthesis of UiO-66, UiO-67 and their derivatives, Chem. Commun., 49 (2013) 9449–9451.
[26] G.C. Shearer, J.G. Vitillo, S. Bordiga, S. Svelle, U. Olsbye, K.P. Lillerud, Functionalizing the defects: post synthetic ligand exchange in the metal organic framework UiO-66, Chem. Mater., 28 (2016) 7190–7193.
[27] G.C. Shearer, S. Chavan, S. Bordiga, S. Svelle, U. Olsbye, K.P. Lillerud, Defect engineering: tuning the porosity and composition of the metal–organic framework UiO-66, Chem. Mater., 28 (2016) 3749–3761.
[28] A.M. Ebrahim, T.J. Bandosz, Ce(III) doped Zr-based MOFs as excellent NO_2 adsorbents at ambient conditions, ACS Appl. Mater. Interfaces, 5 (2013) 10565–10573.
[29] G. Lu, C. Cui, W. Zhang, Y. Liu, F. Huo, Synthesis and self-assembly of monodispersed metal-organic framework microcrystals, Chem. Asian J., 8 (2013) 69–80.
[30] S. Diring, S. Furukawa, Y. Takashima, T. Tsuruoka, S. Kitagawa, Controlled multiscale synthesis of porous coordination polymer in nano/micro regimes, Chem. Mater., 22 (2010) 4531–4538.
[31] L. Zeng, L. Xiao, Y. ke, L. Xiao, w. Shi, Trichloroacetic acid-modulated synthesis of polyoxometalate@UiO-66 for selective adsorption of cationic dyes, J. Colloid Interface Sci., 516 (2018) 274–283.
[32] A. Schaate, Modulated synthesis of Zr-based metal–organic frameworks: from nano to single crystals, Chemistry, 17 (2011) 6643–6651.
[33] Q. Chen, Q. He, M. Lv, Y. Xu, H. Yang, X. Liu, F. Wei, Selective adsorption of cationic dyes by UiO-66-NH_2, Appl. Surf. Sci., 327 (2015) 77–85.
[34] C. Wang, X. Liu, J.P. Chen, K. Li, Superior removal of arsenic from water with zirconium metal–organic framework UiO-66, Sci. Rep., 5 (2015) 16613–16622.
[35] G.C. Shearer, S. Chavan, J. Ethiraj, J.G. Vitillo, S. Svelle, U. Olsbye, C. Lamberti, S. Bordiga, K.P. Lillerud, Tuned to perfection: ironing out the defects in metal–organic framework UiO-66, Chem. Mater., 26 (2014) 4068–4071.
[36] J.M. Yang, A facile approach to fabricate an immobilized-phosphate zirconium-based metal-organic framework composite (UiO-66-P) and its activity in the adsorption and separation of organic dyes, J. Colloid Interface Sci., 505 (2017) 178–185.
[37] P.S. Kumar, S. Ramalingam, C. Senthamarai, M. Niranjanaa, P. Vijayalakshmi, S. Sivanesan, Adsorption of dye from aqueous solution by cashew nut shell: studies on equilibrium isotherm, kinetics and thermodynamics of interactions, Desalination, 261 (2010) 52–60.
[38] J. Abdi, M. Vossoughi, N.M. Mahmoodi, I. Alemzadeh, Synthesis of metal-organic framework hybrid nanocomposites based on GO and CNT with high adsorption capacity for dye removal, Open Chem. Eng. J., 326 (2017) 1145–1158.
[39] P. Ghosh, Y.J. Colón, R.Q. Snurr, Water adsorption in UiO-66: the importance of defects, Chem. Commun., 50 (2014) 11329–11331.
[40] M.K. Purkait, A. Maiti, S. Dasgupta, S. De, Removal of congo red using activated carbon and its regeneration, J. Hazard. Mater., 145 (2007) 287–295.
[41] Q.D. Qin, J. Ma, D.F. Fu, Adsorption of nitrobenzene and benzoic acid from aqueous solution by all-silica zeolite beta, Adv. Mater. Res., 183–185 (2011) 1378–1382.
[42] K. Chai, H. Ji, Dual functional adsorption of benzoic acid from wastewater by biological-based chitosan grafted β-cyclodextrin, Chem. Eng. J., 203 (2012) 309–318.
[43] L. Ai, J. Jiang, Fast removal of organic dyes from aqueous solutions by AC/ferrospinel composite, Desalination, 262 (2010) 134–140.
[44] N.M. Mahmoodi, F. Najafi, Synthesis, amine functionalization and dye removal ability of titania/silica nano-hybrid, Microporous Mesoporous Mater., 156 (2012) 153–160.
[45] B. Zhang, Z. Dong, D. Sun, T. Wu, Y. Li, Enhanced adsorption capacity of dyes by surfactant-modified layered double hydroxides from aqueous solution, J. Ind. Eng. Chem., 49 (2017) 208–218.
[46] M. Aghajanzadeh, M. Zamani, H. Molavi, H.K. Manjili, H. Danafar, A. Shojaei, Preparation of metal–organic frameworks UiO-66 for adsorptive removal of methotrexate from aqueous solution, J. Inorg. Organomet. Polym Mater., 28 (2018) 177–186.
[47] S. Feng, X. Li, F. Ma, R. Liu, G. Fu, S. Xing, X. Yue, Prussian blue functionalized microcapsules for effective removal of cesium in a water environment, RSC Adv., 6 (2016) 34399–34410.
[48] Y.S. Ho, Using of "pseudo-second-order model" in adsorption, Environ. Sci. Pollut. Res., 21 (2014) 7234–7235.
[49] M. Musah, U. Mt, Study of the intraparticle diffusion of Cr (VI), Mn (II) and Cd (II) on modified gold coast bombax, J. Sci. Eng. Res., 5 (2018) 400–408.
[50] M. Ghaedi, A.M. Ghaedi, E. Negintaji, A. Ansari, A. Vafaei, M. Rajabi, Random forest model for removal of bromophenol blue using activated carbon obtained from *Astragalus bisulcatus* tree, J. Ind. Eng. Chem., 20 (2014) 1793–1803.
[51] Q. Jin, L. Huang, A. Li, A. Shan, Quantification of the limitation of Langmuir model used in adsorption research on sediments via site energy heterogeneity, Chemosphere, 185 (2017) 518–528.
[52] J.H. Wang, Y.F. Ji, S.L. Ding, H.R. Ma, X.J. Han, Adsorption and desorption behavior of tannic acid in aqueous solution on polyaniline adsorbent, Chin. J. Chem. Eng., 21 (2013) 594–599.
[53] Z.M. Magriotis, S.S. Vieira, A.A. Saczk, N.A.V. Santos, N.R. Stradiotto, Removal of dyes by lignocellulose adsorbents originating from biodiesel production, J. Environ. Chem. Eng., 2 (2014) 2199–2210.
[54] N.M. Mahmoodi, J. Abdi, F. Najafi, Gemini polymeric nanoarchitecture as a novel adsorbent: synthesis and dye removal from multicomponent system, J. Colloid Interface Sci., 400 (2013) 88–96.
[55] K.Y.A. Lin, W.D. Lee, Self-assembled magnetic graphene supported ZIF-67 as a recoverable and efficient adsorbent for benzotriazole, Chem. Eng. J., 284 (2016) 1017–1027.
[56] Y.J. Kong, L.J. Han, L.T. Fan, F.Z. Kong, X. Zhou, A bismuth-based fluorous metal-organic framework for efficient degradation of Congo red, J. Fluorine Chem., 186 (2016) 40–44.
[57] M.Y. Masoomi, A. Morsali, P.C. Junk, J. Wang, Ultrasonic assisted synthesis of two new coordination polymers and their applications as precursors for preparation of nano-materials, Ultrason. Sonochem., 34 (2017) 984–992.
[58] B. Ding, Y. Cheng, J. Wu, X.M. Wu, H.M. Zhang, Y. Luo, X.F. Shi, X.X. Wu, J.Z. Huo, Y.Y. Liu, A unique multifunctional cluster-based nano-porous Terbium organic material: real-time detection of benzaldehyde, visually luminescent sensor for nitrite and selective high capacity capture of Congo Red, Dyes Pigm., 146 (2017) 455–466.
[59] X.X. Wang, Z.X. Li, B. Yu, K.V. Hecke, G.H. Cui, Synthesis and characterizations of a bis(triazole)-based 3D crystalline copper (II) MOF with high adsorption capacity for congo red dye, Inorg. Chem. Commun., 54 (2015) 9–11.
[60] J. Hu, H. Yu, W. Dai, X. Yan, X. Hu, H. Huang, Enhanced adsorptive removal of hazardous anionic dye "congo red" by a Ni/Cu mixed-component metal–organic porous material, RSC Adv., 4 (2014) 35124–35130.
[61] S. Zhao, D. Chen, F. Wei, N. Chen, Z. Liang, Y. Luo, Removal of Congo red dye from aqueous solution with nickel-based metal-organic framework/graphene oxide composites prepared by ultrasonic wave-assisted ball milling, Ultrason. Sonochem., 39 (2017) 845–852.
[62] S. Feng, F. Ma, R. Liu, S. Li, X. Li, Y. Jin, G. Fu, X. Yue, Highly efficient removal of trace level dieldrin from water resource utilizing a cerasomal strategy, J. Mater. Chem. A, 26 (2016) 10263–10273.
[63] M. Kara, H. Yuzer, E. Sabah, M.S. Celik, Adsorption of cobalt from aqueous solutions onto sepiolite, Water Res.,37 (2003) 224–232.